ENGINEERING TRANSACTIONS • *Engng. Trans.* • **61**, 3, 173–184, 2013
Polish Academy of Sciences • Institute of Fundamental Technological Research (IPPT PAN)
National Engineering School of Metz (ENIM)

Structural Behavior of Sandwich Panels with External Deep-Profiled and Internal Soft Facing

Zbigniew POZORSKI[1)], Rafał SÓL[1)], Jacek SZAJDA[1)], Jolanta BŁASZCZUK[2)]

[1)] *Poznan University of Technology, Institute of Structural Engineering*
Piotrowo 5, 60-965 Poznań, Poland
e-mail: zbigniew.pozorski@put.poznan.pl

[2)] *Czestochowa University of Technology, Institute of Mathematics*
Armii Krajowej 21, 42-200 Częstochowa, Poland

Sandwich panels made of deep-profiled steel facesheet, thick and soft PUR core and thin aluminum facesheet are considered. The structural behavior of the panel in two arrangements is analyzed by the way of real experiments. Three-point bending tests were carried out. The laboratory tests unraveled non-linear characteristics of structural behavior. The local instability of the compressed faces was observed. The real experiments were compared with the results of numerical simulations.

Key words: sandwich panels, PUR core, soft facing, experimental analysis, three-point bending, failure mechanisms.

1. Introduction

Sandwich panels which are utilized in civil engineering usually consist of thin and rigid (often deep-profiled) external facings and a thick and soft core. They are used as roof and wall cladding. Lately, sandwich panels with one face soft instead of rigid have aroused wide interest. The soft face can be made of composite paper, aluminum, elastic fibres or other materials. In spite of difficulties in production and limitations in typical applications, the producers have new product applications in view. Certainly they are also motivated by lower costs of production.

A general review of sandwich structure problems was presented by Zenkert [16] and Davies [4], while a survey of failure modes was given by Daniel *et al.* [3]. The most important aspects of structural behavior of sandwich panels are: shear deformability of the core, creep of the core, and local instability

(wrinkling) of compressed facing. Theories concerning shear deformable beams and plates are presented in [14]. The problem of creep of beams with polymer foam cores was discussed in [6].

The classical experimental approach to the wrinkling stress assessment was presented in [5]. The paper discusses the results of 3-point bending, 4-point bending laboratory tests and column compression tests. The extensive analysis of failure modes of sandwich beams was presented in [12]. This study focused on the competing collapse mechanisms for simply supported sandwich beams subjected to 3-point bending. The analysis of sandwich structure with a specific core type, namely metallic foam core, was investigated in [10]. This kind of foam can fail by several modes.

The influence of geometrical and mechanical parameters on the non-linear behavior of sandwich structures is usually studied by numerical and analytical simulations. It was presented in [9] that sandwiches are very sensitive to geometrical imperfections. The extensive parametric simulations of sandwich beams under pure bending (4-point bending) are presented in [7]. In particular, the influence of the core depth and core mechanical parameters on wrinkling failure was analyzed. Classical experimental methods often fail in the case of strongly localized effect analysis. Therefore, new methods of investigations are proposed. The application of the photoelastic method to local effects evaluation is presented in [13]. The method allows one to assess local stress concentration and the influence of the indentation process.

In sandwich structures with the soft core the shear rigidity of the panel plays a crucial role. A group of identification methods of the shear modulus of the core was described in [8]. The new method of determination of the shear rigidity was proposed in [1, 2]. The proper determination of mechanical parameters highly influences the accuracy of the prediction of sandwich structure behavior. Therefore, new and more sophisticated methods are still investigated [15].

To our surprise we found a lack of papers that concern the behavior of sandwich structures with external soft face. Static analysis of sandwich structures with one soft face is a challenge. Ordinary sandwich panel theory is not reliable in such a case because of the susceptibility of the soft facesheet. From an other point of view, treatment of the structure as a deep-profiled steel sheet with additional thermal insulation and omission of the influence of the soft face leads to improper simplifications.

2. Experimental tests

To examine sandwich panel behavior under loading, 3-point bending tests were performed. Two situations were taken into consideration. In the first case

the panel is arranged with the deep-profiled steel facesheet on the top and soft face on the bottom. The steel face is subjected to bending and compression whereas the soft face is under tension. In the second case, the panel is lying with the soft face on top. This case should result in the compression of the aluminum soft face and combination of bending and tension of deep-profiled steel facesheet. The value of the excitation force, the strains in both faces, and the displacements of the plate were measured during all the tests.

2.1. Panel geometry

Figure 1 presents the cross-section of the panel. The deep-profiled face is made of zinc-galvanized steel. The measured steel core thickness is 0.395 mm, whereas the nominal yield stress of the steel is 280 MPa. The real yield stress is even higher and equals about 350 MPa. The steel is covered by a zinc layer (zinc total thickness 0.026 mm). The thickness of the internal aluminum face is 50 μm. The PUR core thickness is equal to 40 mm in the valley and 80 mm in the rib.

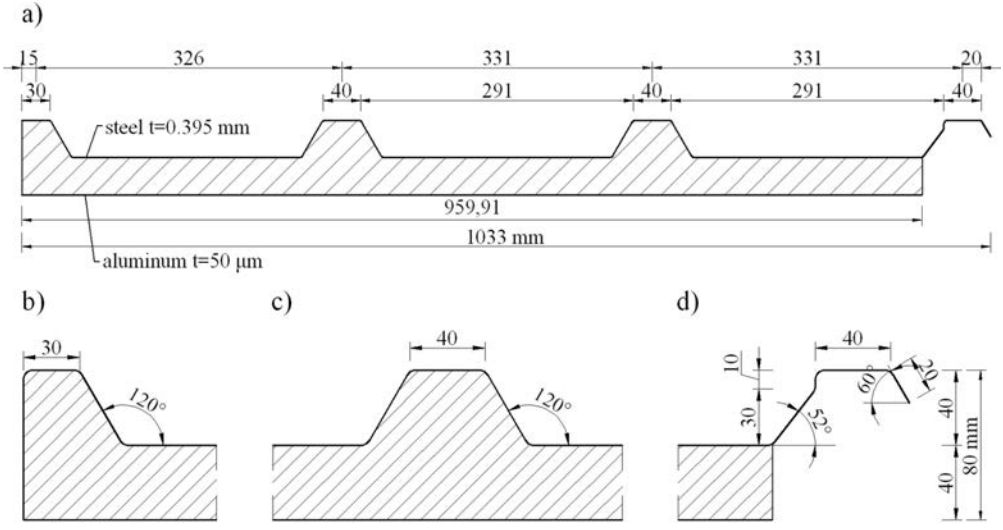

FIG. 1. The cross-section of the panel: a) overview, b) filled rib, c) rib profiling, d) free edge (longitudinal steel profiling without foam filling of the rib).

The tests were carried out on full width specimens (Fig. 1a). The total length of the panel was equal to 2.0 m. This length was chosen to provide bending failure, but the influence of the core shear is also significant. The width of the supports was 100 mm, giving the span length equal to $L = 1.90$ m. The static system is shown in Fig. 2.

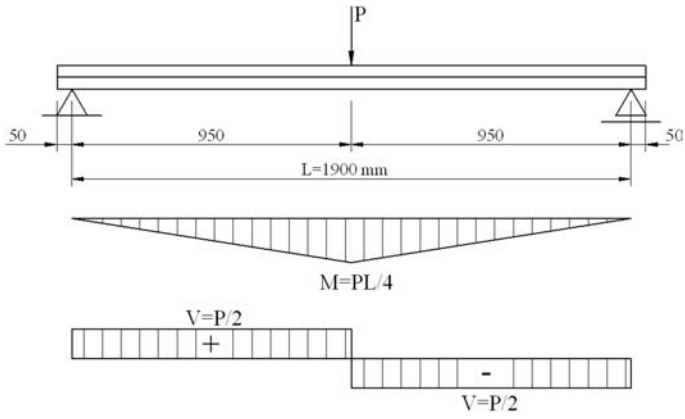

FIG. 2. The static system of the experiment (3-point bending test).

2.2. Apparatus

The test-bench consists of supporting and loading systems, force and strain gauges, and displacement transducers. The force was excited by the hydraulic jack and transferred to the panel through the loading beam. The force values were registered using the HBM C6A 50 kN load cell installed directly under the jack. Strains were measured on the both faces by HBM 10/120 LY41 linear

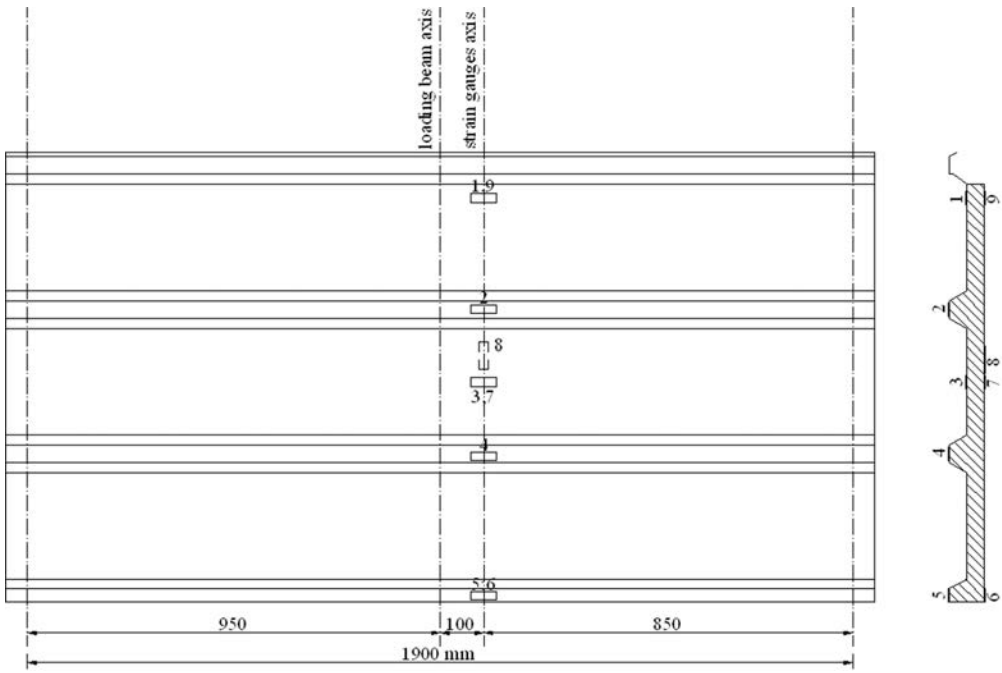

FIG. 3. The location of strain gauges.

strain gauges. All strain gauges were located at a distance of 100 mm from the loading beam axis. It limits the influence of local effects (e.g. indentation) on the strain measurements. The location of the strain gauges is specified in Fig. 3. The strain gauge numbers 1, 3 and 2, 4, 5 were placed in the valleys and on the ribs of the deep-profiled face, respectively. The strain gauge numbers 6, 7, 9 were placed on the aluminum face. Additionally, the strain gauge number 8 measured the strain of the aluminum face in the direction parallel to the loading line. The displacement transducers were mounted at both edges of the panel, in the distant 100 mm from the middle of the panel.

2.3. Situation 1 – the deep-profiled steel face on the top

In this panel arrangement the damage is related to the wrinkling of the steel ribs under compression (Fig. 4a). Tension failure of the aluminum face, and panel breakage, took place subsequently (Fig. 4b). Figure 5 shows the force-

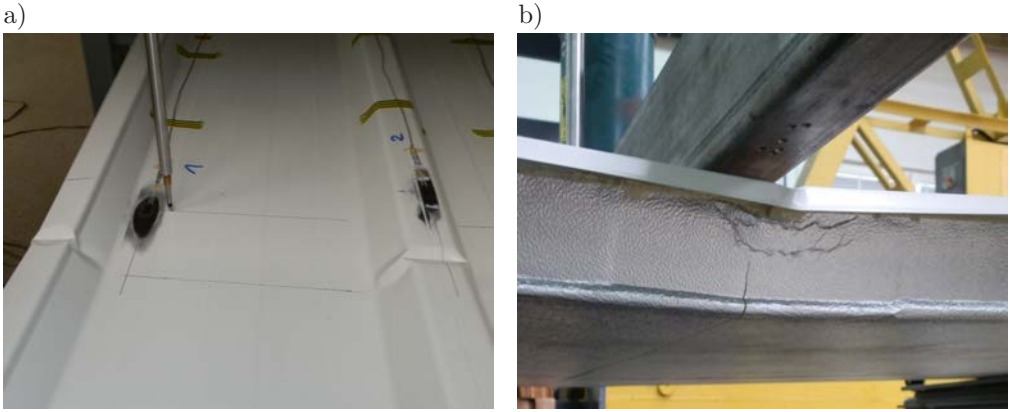

FIG. 4. The damage mechanism in situation 1: a) wrinkling of the deep-profiled steel face, b) aluminum face failure.

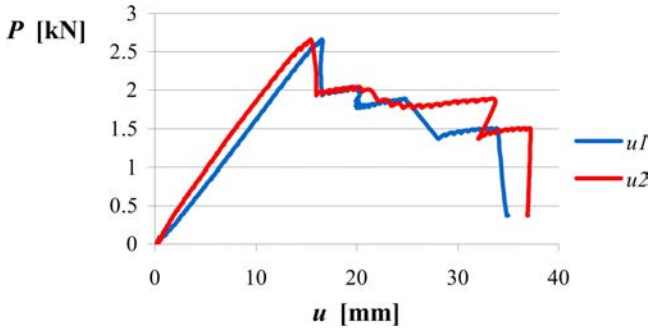

FIG. 5. The force-displacement relation in situation 1; $u1$ – the displacement measured next to the free edge of face profiling, $u2$ – the displacement measured next to the filled rib, displacement limit $L/150 = 12.67$ mm.

displacement relation in this situation. This relation is almost linear until the damage occurs. The panel displacement at the peak force $P_{\max} = 2.66$ kN is equal to 16.54 mm, which exceeds the displacement limit, $u_{\lim} = L/150 = 12.67$ mm.

To estimate the stress level in the facesheets, several assumptions were made:

- Young's modulus of the steel face is 210 GPa,
- Young's modulus of the aluminum face is 70 GPa,
- the linear part of the strain-stress relation can be expressed by Hooke's law.

The strains in the upper region of the steel face reached $\varepsilon = -0.00138$ at maximum load (Fig. 6). It corresponds to the compression stress −289.8 MPa. This means that the wrinkling stress is a little bit higher than the declared yield stress.

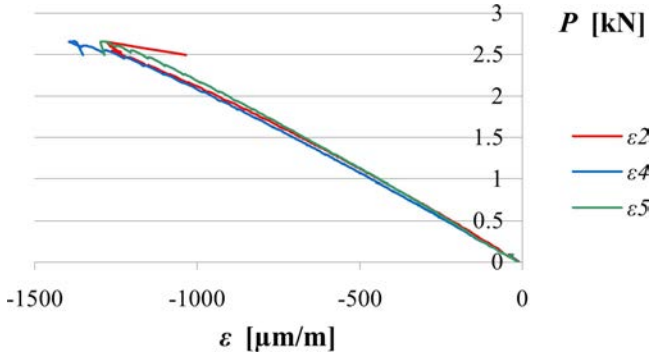

FIG. 6. Strains on the top of steel face in situation 1.

The strain in the aluminum face at a peak force $P_{\max} = 2.66$ kN was $\varepsilon = 0.00125$. Assuming Hooke's law, this gives stress 87.5 MPa. The strain measured at the moment of the tension failure was equal to $\varepsilon = 0.00306$. Figure 6 presents the estimated stress distribution within the cross-section of the panel for the peak load $P_{\max} = 2.66$ kN. Note that neither dead load nor apparatus weight were included. The additional bending moment caused by them was equal to 0.179 kNm.

The stress distribution was assessed using the measured values of strains. It needs to be emphasized that following the classical sandwich panel theory [4, 16], contrary to the classical Bernoulli beam theory, the strain distribution is not linear. The cross-section, which is initially plane, does not remain plane after deformation. The cross-section deformation is described by the superposition of the rotation of the normal element and the shear deformation of the core.

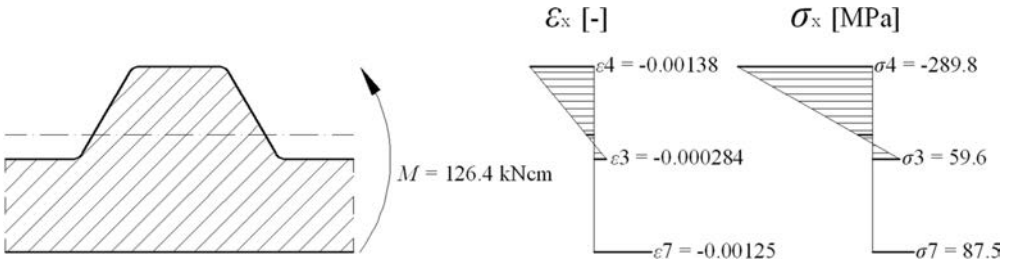

FIG. 7. The measured strains values and estimated stress distribution for $P = 2.66$ kN in the situation 1 (assuming $\sigma = E\varepsilon$).

2.4. Situation 2 – aluminum soft face on the top

In this case the failure mechanism is initiated by yielding of the tensioned part of the deep-profiled steel face. At the same time the foam core is locally deformed by the line loading. The thin aluminum paper is pressed down into the core (Fig. 8a). Since the deep-profiled facesheet is subjected to bending, the valleys of the cross-section are compressed. A high level of compression finally leads to the local instability of compressed parts of the steel facesheet (Fig. 8b).

a) b)

FIG. 8. The damage mechanism in situation 2: a) local core crushing due to line loading, b) wrinkling of the steel face in the valleys.

The force-displacement relation is evidently non-linear (Fig. 9). The displacement registered at a peak force of 3.32 kN was equal to 29.06 mm. Non-linearity occurred at the load level greater than 2.0 kN. Up to this force the displacements in both cases are comparable (situation 1: $u(P = 2.0\text{ kN}) = 11.57$ mm; situation 2: $u(P = 2.0\text{ kN}) = 12.06$ mm).

The strain in the outer part of the steel facesheet reached $\varepsilon = 0.00190$. Multiplying the strain by the Young modulus, the tensile stress 399.0 MPa is achieved,

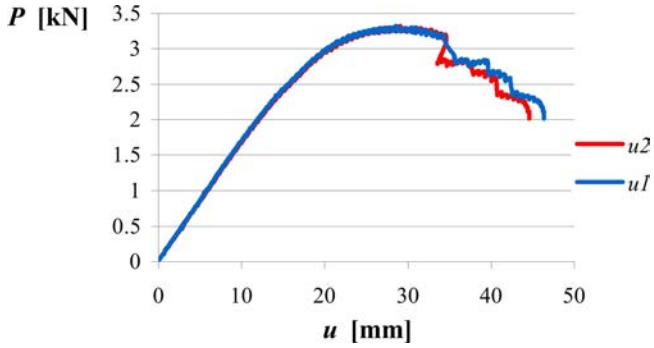

FIG. 9. The force-displacement relation in situation 2: $u1$ – the displacement measured next to the filled rib, $u2$ – the displacement measured next to the free edge of face profiling, displacement limit $L/150$=12.67 mm.

which exceeds the yield stress. More probable is a lower stress value. The strain in the compressed part of the steel face equalled $\varepsilon = -0.00080$, which corresponds to the compression stress -168.0 MPa. The measured aluminum face strain was $\varepsilon = -0.000795$, although this value is questionable. The estimated stress distribution is shown in Fig. 10.

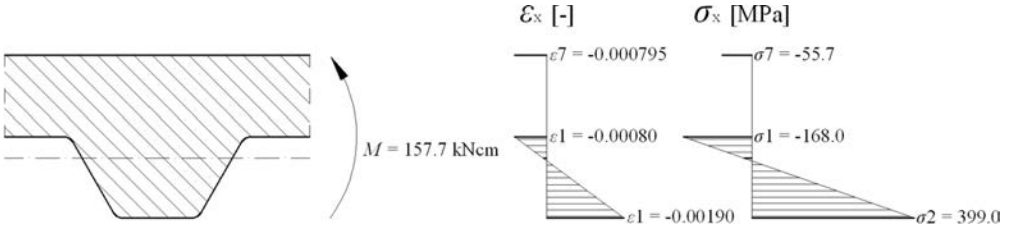

FIG. 10. The estimated stress distribution for P=3.32 kN in situation 2 (assuming $\sigma = E\varepsilon$).

The stress value in the aluminum facesheet is dubious, because there were some difficulties in attaching the strain gauges to the aluminum face. Cement that was used showed greater stiffness than the aluminum paper itself, which certainly had the influence on the experimental results.

3. Numerical simulations

3.1. Numerical model

The parameters of the numerical simulations strictly correspond to the real experiments. The simulations were prepared in the ABAQUS system environment. All materials were assumed as elastic, but also the case of elastic – ideal plastic model of steel and aluminum materials was taken into account. The core

was assumed as elastic because the extreme normal stress is in the linear range ($65.7 < 120$ kPa). Material parameters that were used are listed in Table 1. The deep-profiling facing has the thickness 0.421 mm, the resultant Young's modulus of this face is equal to $E = 202.2$ GPa and includes the influence of the zinc layer ($t_{\text{steel}} = 0.395$ mm, $E_{\text{steel}} = 210$ GPa, $t_{\text{zinc}} = 0.026$ mm, $E_{\text{zinc}} = 84$ GPa). Both faces were modeled using four nodes, doubly curved, thin or thick shell, reduced integration, and hourglass control, finite membrane strain elements S4R. The core of the panel was modeled using eight node linear brick elements C3D8R. Interactions between all parts were defined as TIE type, which makes equal displacements of nodes.

Table 1. Properties of materials used in numerical analysis.

Part	Young's modulus	Poisson's ratio	Yield stress
Steel face	202.2 GPa	0.30	350 MPa
PUR core	8.00 MPa	0.05	–
Aluminum face	70.0 GPa	0.33	95 MPa

3.2. Comparison of the results of experiments and FEM analysis

The panel displacements $u1$ and $u2$, as well as the strains at nine chosen points at different load levels, were compared. Strain values, which were taken from the numerical simulations, correspond to the localization of the strain gauges (Fig. 3). Comparisons of experimental and numerical data in both situations are presented in Table 2 and 3. The strains in the steel facesheet, which are crucial for sandwich structure load-bearing capacity, have satisfying accuracy with the experiments. The great divergence of the strains in aluminum face could be caused by several factors. First of all, accurate material properties of aluminum paper were unknown. Secondly, the cement, which was used to attach the strain gauges, had significant stiffness compared to the stiffness of the aluminum paper. Finally, the most difficult phenomenon for proper numerical estimation is the local instability of compressed, very thin, and geometrically imperfect aluminum face.

The comparisons of the strains ε as the function of the loading force P for the real experiment and numerical simulations are shown in Fig. 11 and 12. The comparisons concern situation 1 (the deep-profiled steel face on the top in the compression), the strains in the valley (point 3, Fig. 11), and on the rib (point 4, Fig. 12). The relations are almost linear, only the behavior for load greater than 2.0 kN is nonlinear. The nonlinearity is observed in the real results and in the numerical solution for the point located in the valley, in the case of the elastic-plastic definition of the materials ($\varepsilon 3$ pl).

Table 2. Comparison of the experimental and numerical results in the situation 1.

	P [kN]	$u1$ [mm]	$u2$ [mm]	Strain in the steel face ($\cdot 10^4$)					Strain in the alu ($\cdot 10^4$)			
				$\varepsilon 1$ [–]	$\varepsilon 2$ [–]	$\varepsilon 3$ [–]	$\varepsilon 4$ [–]	$\varepsilon 5$ [–]	$\varepsilon 6$ [–]	$\varepsilon 7$ [–]	$\varepsilon 8$ [–]	$\varepsilon 9$ [–]
Exp.	1.00	5.93	5.45	1.17	−4.44	1.04	−4.66	−4.43	3.09	4.46	0.321	3.26
Num.	1.00	4.98	4.73	1.37	−4.91	1.14	−4.77	−4.14	6.02	6.01	−0.112	6.22
Δ[%]*		−15.9	−13.3	16.7	10.4	9.4	2.3	−6.5	94.7	34.8	−65.2	90.8
Exp.	2.50	14.78	14.55	3.15	−12.4	2.66	−12.5	−11.8	7.44	11.4	0.238	8.84
Num.	2.50	12.46	11.81	3.42	−12.3	2.84	−11.9	−10.4	15.1	15.0	−0.279	15.5
Δ[%]*		−15.7	−18.8	8.5	−0.8	6.7	−4.7	−11.9	102.3	31.8	17.2	75.9

*Δ = (|exp data| − |num data|)/|exp data|

Table 3. Comparison of the experimental and numerical results in the situation 2.

	P [kN]	$u1$ [mm]	$u2$ [mm]	Strain in the steel face ($\cdot 10^4$)					Strain in the alu ($\cdot 10^4$)			
				$\varepsilon 1$ [–]	$\varepsilon 2$ [–]	$\varepsilon 3$ [–]	$\varepsilon 4$ [–]	$\varepsilon 5$ [–]	$\varepsilon 6$ [–]	$\varepsilon 7$ [–]	$\varepsilon 8$ [–]	$\varepsilon 9$ [–]
Exp.	1.00	5.81	5.68	−1.53	4.69	−0.96	4.57	4.47	−4.92	−4.23	−0.221	−2.96
Num.	1.00	4.32	4.67	−1.16	4.32	−1.02	4.50	4.20	−7.47	−6.54	0.024	−7.25
Δ[%]*		−25.7	−17.8	−24.1	−7.8	6.0	−1.5	−6.0	52.0	54.7	−89.1	145.1
Exp.	3.00	20.49	20.20	−6.28	17.4	−3.41	17.2	17.3	−10.1	−8.85	−2.41	−3.62
Num.	3.00	12.95	14.02	−3.48	13.0	−3.06	13.5	12.6	−22.4	−19.6	0.072	−21.8
Δ[%]*		−36.8	−30.6	−44.6	−25.5	−10.2	−21.6	−27.0	122.4	121.7	−97.0	500.4

*Δ = (|exp data| − |num data|)/|exp data|

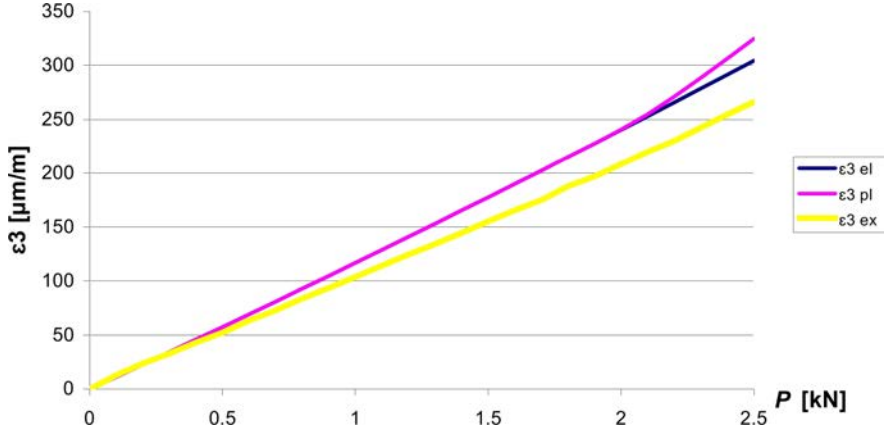

FIG. 11. The relation $\varepsilon(P)$ for the point 3 located in the valley: $\varepsilon 3$ ex – experimental results, $\varepsilon 3$ el – numerical results, elastic materials, $\varepsilon 3$ pl – numerical results, elastic-plastic materials.

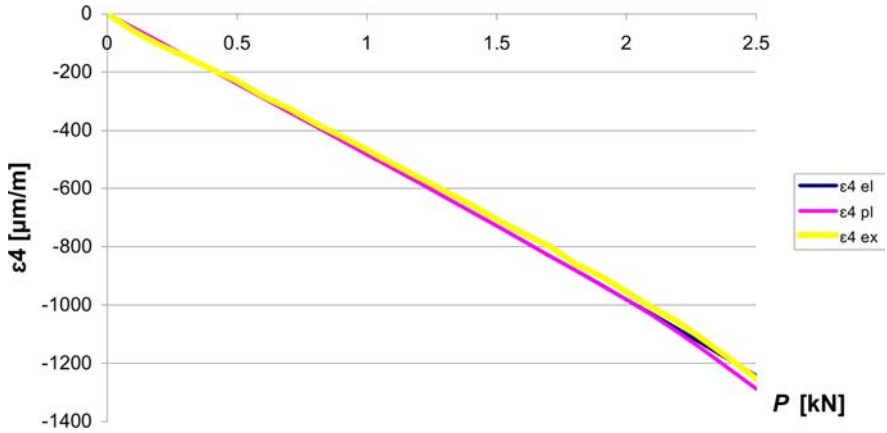

FIG. 12. The relation $\varepsilon(P)$ for the point 4 located on the rib: $\varepsilon 4$ ex – experimental results, $\varepsilon 4$ el – numerical results, elastic materials, $\varepsilon 4$ pl – numerical results, elastic-plastic materials.

4. CONCLUSIONS

The presented results show that behavior of sandwich panels with one rigid and one soft face is very interesting. The failure mechanism depends on the arrangement of the panel. In the case of a compressed deep-profiled steel face the damage is related to the wrinkling of the steel ribs. In the case of the aluminum soft face on the top, the failure is initiated by yielding of the steel face and the local foam core crushing. Finally, bending of the structure leads to the local instability of the compressed part (valley) of the steel facesheet.

From the practical point of view, better results were achieved in the case of the deep-profiled face located on the bottom. The limit load is higher in this case by about 20% and the range of nonlinear behavior is broader. It is the opinion of the authors, that such a system is safer. The enhancement of the carrying capacity is possible by increasing of the steel face rigidity (thicker face, more ribs, deeper profiling) or application of the second stiff facesheet instead of soft aluminum paper. Unfortunately, all these operations cause an increase of the costs of the panel production.

Contrary to all expectations, the bending capacity of the analyzed structure with the soft face is much higher than the capacity of the pure steel profile. According to FEM analysis presented in [11], the bending capacity of sandwich structure with soft face is at least 25% higher than the capacity of steel profile itself, not to mention about greater stiffness and higher thermal insulation. Conducted experiments indicate that soft core and soft aluminum face cooperate with the deep-profiled steel face. It encourages applying such panels as the roof covering with an additional waterproof layer placed on the top of the sandwich.

References

1. Chuda-Kowalska M. *et al.*, *Experimental determination of shear rigidity of sandwich panels with soft core*, Proc. of 10th International Conference Modern Buildings Materials, Structures and Techniques, Vol. I, P. Vainiunas and E.K. Zavadskas [Eds.], Vilnius, Lithuania, VGTU, 56–63, 2010.
2. Chuda-Kowalska M., Garstecki A., *Determination of materials constants for sandwich panels with PUR core* [in Polish: *Wyznaczanie stałych materiałowych dla płyt warstwowych z rdzeniem PUR*], Przegląd budowlany, **3**, 67–72, 2012.
3. Daniel I.M., Gdoutos E.E., Wang K.-A., Abot J.L., *Failure modes of composite sandwich beams*, Int. J. Damage Mechanics, **11**, 309–334, 2002.
4. Davies J.M., *Light Weight Sandwich Construction*, Blackwell Science, 2001.
5. Gdoutos E.E., Daniel I.M., Wang K.-A., *Compression facing wrinkling of composite sandwich structures*, Mechanics of materials, **35**, 511–522, 2003.
6. Huang J.S. *et al.*, *Creep of sandwich beams with polymer foam cores*, Journal of Materials in Civil Engineering, **2**, 3, 171–182, 1990.
7. Jasion P., Magnucki K., *Face wrinkling of sandwich beams under pure bending*, Journal of Theoretical and Applied Mechanics, **50**, 4, 933–941, 2012.
8. Juntikka R., Hallstorm S., *Shear characterization of sandwich core materials using four-point bending*, Journal of Sandwich Structures and Materials, **9**, 1, 67–94, 2007.
9. Léotoing L., Drapier S., Vautrin A., *Nonlinear interaction of geometrical and material properties in sandwich beam instabilities*, Int. J. Solid and Structures, **39**, 3717–3739, 2002.
10. McCormack T., Miller R., Kesler O., Gibson L., *Failure of sandwich beams with metallic foam cores*, Int. J. of Solids and Structures, **38**, 4901–4920, 2001.
11. Sól R., Szajda J., *Stress and strain analysis in sandwich panels with one metal facing subjected to bending* [in Polish: *Analiza stanu naprężenia i odkształcenia w zginanych płytach warstwowych z jednostronną okładziną stalową*], Poznan University of Technology, 2012.
12. Steeves C.A., Fleck N.A., *Collapse mechanisms of sandwich beams with composite faces and a foam core, loaded in three-point bending. Part II: experimental investigation and numerical modelling*, Int. J. of Mechanical Sciences, **46**, 585–608, 2004.
13. Thomsen O.T., Frostig Y., *Localized bending effects in sandwich beams: photoelastic investigations versus high-order sandwich theory results*, Composite Structures, **37**, 97–108, 1997.
14. Wang C.M., Reddy J.N., Lee K.H., *Shear deformable beams and plates*, Elsevier, 2000.
15. Zang S., Dulieu-Barton J.M., Fruehmann R.K., *A methodology for obtaining material properties of polymeric foam at elevated temperatures*, Experimental Mechanics, **52**, 1, 3–15, 2012.
16. Zenkert D., *An Introduction to sandwich construction*, Chameleon Press Ltd., London, 1995.

Received February 13, 2013; revised version March 21, 2013.